PROPAGATION OF SYSTEMATIC ERRORS IN A ONE LAYER PRIMITIVE-EQUATION MODEL FOR SYNOPTIC SCALE MOTION

WILLIAM S. IRVINE, JR,[1] and DAVID D. HOUGHTON

Department of Meteorology, The University of Wisconsin, Madison, Wis.

ABSTRACT

A one-layer, mid-latitude, beta-plane channel model of an incompressible homogeneous fluid is constructed to study the propagation of systematic errors on a nearly stationary synoptic scale wave. A time- and space-centered difference scheme is used to evaluate the governing primitive equations. Data fields resulting from height field perturbations injected at various locations in the synoptic wave are compared to the unperturbed synoptic wave at 3-hr intervals for 5 model days. Results show that the low-frequency or quasi-geostrophic component of the error tends to move toward the core of maximum velocity in the basic state and that, after 5 days, these maximum height errors are in the core regardless of the location of the initial perturbation.

1. INTRODUCTION

Recent years have found atmospheric numerical models becoming more sophisticated. Multilayered models, ultra-high-speed computers, and improved direct observational networks have made accurate global numerical models a reality. One inherent limit to the accuracy of these models, however, is the availability of initializing information. Direct observational data are lacking from large areas of the globe—such as oceans, deserts, the polar regions, and the Tropics.

Recent interest has centered on augmentation of existing direct data networks using satellite information. Johnson (1967) and Smith (1967) have proposed schemes to augment available wind and temperature data using satellite photographs and radiation measurements. While this improved data coverage is desirable, preparing these additional data for numerical model use presents some novel problems.

Model initialization of single-source data has been investigated by Rossby (1938), Houghton and Washington (1969), and others. This work will investigate one special problem associated with initialization of multiple-source data—that of systematic error propagation. Attention is directed primarily to the low-frequency (synoptic scale) motions, although the high-frequency gravity wave modes are also present.

This study has a direct relationship to the problem of predictability. Previous studies by Lorenz (1969a) and Smagorinsky (1969) have considered the effect of initial errors or deviations on a forecast in terms of statistical comparisons involving the entire integration domain. In this study, the comparison is in terms of actual difference maps which can demonstrate the variation in predictability that exists as a function of location. The analysis provides information on the horizontal propagation of information or energy in a simple atmosphere. Knowledge of energy propagation in the atmosphere is fundamental to understanding the complicated interactions of atmospheric motions. In numerical models, there is the additional related problem of error propagation from any artificial boundaries.

This study uses a simple one-layer model to perform numerous experiments using variations of one basic initial condition. One-layer modeling has the advantages of economy and simplicity. Shuman (1962), Houghton and Kasahara (1968), and many others have taken advantage of these features to study atmospheric problems as varied as synoptic scale motions and mountain flow. While one-layer models are unrealistic descriptions of certain conditions, such as deep convection and baroclinic development, one may assume that general conclusions can be made applicable to certain modes of multilayer models (and perhaps the real atmosphere).

This study will describe a one-layer model and a series of seven experiments involving a typical synoptic scale wave. A synoptic scale wave with negligible east-west trace velocity is run in the model for 5 days. This wave is used as a standard for comparison with six additional experiments. These additional experiments are identical to the first except for a small initial height perturbation located in or near the core of maximum fluid velocity. Conclusions are then made as to the sensitivity of the basic flow to the injection of this small perturbation at six locations.

Injecting height perturbations into a basic flow is intended to simulate the incorporation of asynoptic data into a synoptic data network. Here, asynoptic data such as satellite data are expected to exhibit some systematic deviation from conventional data over the entire initial data field. Section 2 describes the model characteristics and the basic equations. In section 3, the stability criteria (both physical and numerical) are discussed. The initialization procedures are given in section 4, and the numerical experiments are described in section 5. Finally, experi-

[1] Now affiliated with Air Force Global Weather Central, Offutt Air Force Base, Nebr.

mental results and conclusions of the study are presented in section 6.

2. MODEL CHARACTERISTICS AND BASIC EQUATIONS

The model used for this study is a mid-latitude channel model of an incompressible homogeneous fluid. The lower surface is rigid and flat, the upper surface is free. The northern and southern boundaries are rigid vertical walls where the north-south velocity, V, is constrained to vanish. The flow is made periodic in the east-west direction with a wavelength of 6720 km. The model has the same dimensions and equally spaced grid points in both horizontal directions. The Coriolis parameter is evaluated from a beta plane centered at 45°N.

For reducing the speed of gravity wave propagation and to simulate motion in the troposphere rather than the entire atmosphere, an inert fluid of infinite depth is placed above the free surface. This effect, described by Houghton et al. (1966), is achieved in actuality by "reducing" gravity in this study from 9.8 to 1.4 m/s².

The model is initialized by prescribing a stream function. The three dependent variables (height and east-west and north-south fluid velocity) are determined by using balance and quasi-geostrophic divergence relationships, discussed further in section 4. Time integration using Grammeltvedt's scheme F (1969), as formulated in this section, proceeds for 5 days. The model disturbance energy is calculated at each time step to check conservation of total energy, and the three dependent variables are made available at 3-hr intervals.

Symbols used frequently in this work are

f Coriolis parameter,
g reduced acceleration of gravity,
h depth of the fluid,
i index parameter in the x direction,
j index parameter in the y direction,
M number of grid points in the x direction,
N number of grid points in the y direction,
t time,
U,V velocity components in the x and y directions,
x,y east-west and north-south Cartesian coordinates,
ρ fluid density (constant),
χ velocity potential, and
ψ stream function.

The basic Eulerian equations are

$$\frac{\partial U}{\partial t}+U\frac{\partial U}{\partial x}+V\frac{\partial U}{\partial y}-fV+g\frac{\partial h}{\partial x}=0, \qquad (1)$$

$$\frac{\partial V}{\partial t}+U\frac{\partial V}{\partial x}+V\frac{\partial V}{\partial y}+fU+g\frac{\partial h}{\partial y}=0, \qquad (2)$$

and

$$\frac{\partial h}{\partial t}+\frac{\partial(hU)}{\partial x}+\frac{\partial(hV)}{\partial y}=0. \qquad (3)$$

These equations can be rewritten in an alternate form to be used for finite differencing as

$$\frac{\partial U}{\partial t}+\frac{\partial(U^2)}{\partial x}+\frac{\partial(UV)}{\partial y}-U\left(\frac{\partial U}{\partial x}+\frac{\partial V}{\partial y}\right)-fV+g\frac{\partial h}{\partial x}=0, \qquad (4)$$

$$\frac{\partial V}{\partial t}+\frac{\partial(UV)}{\partial x}+\frac{\partial(V^2)}{\partial y}-V\left(\frac{\partial U}{\partial x}+\frac{\partial V}{\partial y}\right)+fU+g\frac{\partial h}{\partial y}=0, \qquad (5)$$

and

$$\frac{\partial h}{\partial t}+\frac{\partial(hU)}{\partial x}+\frac{\partial(hV)}{\partial y}=0. \qquad (6)$$

The integration scheme used for this model is based on Grammeltvedt's scheme F (1969). This scheme has the advantage of conserving total momemtum in the nonlinear terms. With his notation, the scheme can be written as

$$\overline{U}_t^t+(\overline{U}^x\overline{U}^x)_x+(\overline{U}^y\overline{V}^y)_y-U(\overline{U}_x^x+\overline{V}_y^y)-fV+g\overline{h}_x^x=0, \qquad (7)$$

$$\overline{V}_t^t+(\overline{U}^x\overline{V}^x)_x+(\overline{V}^y\overline{V}^y)_y-V(\overline{U}_x^x+\overline{V}_y^y)+fU+g\,\overline{h}_y^y=0, \qquad (8)$$

and

$$\overline{h}_t^t+(\overline{h}^x\overline{U}^x)_x+(\overline{h}^y\overline{V}^y)_y=0. \qquad (9)$$

If α and β are general variables, the operators found in eq (7-9) can be defined as

$$\Delta=\Delta x,\ \Delta y,\ \Delta t,$$

$$\overline{\alpha}_x^x=\frac{1}{2\Delta}\,[\alpha(x_i+\Delta)-\alpha(x_i-\Delta)],$$

$$\overline{\alpha}^{2x}=\frac{1}{2}[\alpha(x_i+\Delta)+\alpha(x_i-\Delta)],$$

and

$$(\overline{\alpha}^x\overline{\beta}^x)_x=\frac{1}{2}\,[\overline{\alpha}^{2x}\overline{\beta}_x^x+\overline{\beta}^{2x}\overline{\alpha}_x^x+\alpha\overline{\beta}_x^x+\beta\overline{\alpha}_x^x].$$

The finite-difference form of the governing equations all contain space- or time-centered approximations to the first derivative terms except at the northern and southern boundaries. Here, because centered space differences in the north-south direction are not possible, one-sided differences must be used. This noncentered space difference has a noticeable but very small effect on the available energy of the model. This was shown by tests using various channel shapes.

The total energy of the model, E, can be expressed as the sum of kinetic and potential energy. Total energy, evaluated over the entire volume of the model can be expressed as

$$E=K\sum_{i=1}^{M}\sum_{j=1}^{N}\,[(U_{i,j}^2+V_{i,j}^2)\,h_{i,j}+gh_{i,j}^2]$$

for the finite-difference model where

$$K=\frac{\rho}{2}(M\Delta x)(N\Delta y)$$

and subscripts refer to grid position, for example,

$$U_{i,j}=U(i\Delta x, j\Delta y).$$

Total disturbance energy (DE) can be evaluated by subtracting the minimum possible potential energy from the total energy of the system:

$$DE=E-Kg\bar{h}^2;$$

or in finite-difference form,

$$DE=K\sum_{i=1}^{M}\sum_{j=1}^{N}[h_{i,j}(U_{i,j}^2+V_{i,j}^2+gh_{i,j})-g\bar{h}^2] \quad (10)$$

where

$$\bar{h}=\frac{1}{MN}\sum_{i=1}^{M}\sum_{j=1}^{N}(h_{i,j}).$$

Disturbance energy is a more sensitive indicator of energy changes of the model than the total energy and will be used throughout this paper to monitor the energy characteristics of the model.

3. STABILITY

Stability, both computational and physical, is investigated for the model equations and basic flow. Conditions for computational stability may be established by taking the basic model equations in Eulerian form, nondimensionalizing and linearizing to form

$$\frac{\partial U'}{\partial t}+\hat{U}\frac{\partial U'}{\partial x}+\hat{V}\frac{\partial U'}{\partial y}+\hat{C}\frac{\partial h'}{\partial x}-fV'=0, \quad (11)$$

$$\frac{\partial V'}{\partial t}+\hat{U}\frac{\partial V'}{\partial x}+\hat{V}\frac{\partial V'}{\partial y}+\hat{C}\frac{\partial h'}{\partial y}+fU'=0, \quad (12)$$

and

$$\frac{\partial h'}{\partial t}+\frac{\partial(h'\hat{U}+\hat{C}U')}{\partial x}+\frac{\partial(h'\hat{V}+\hat{C}V')}{\partial y}=0 \quad (13)$$

where the transformations made are

$$U\rightarrow\hat{U}+\hat{C}U',$$

$$V\rightarrow\hat{V}+\hat{C}V',$$

$$h\rightarrow\hat{H}+\hat{H}h',$$

and

$$\hat{C}=\sqrt{g\hat{H}}$$

where $\hat{U}$, $\hat{V}$, $\hat{H}$, and $\hat{C}$ are basic characteristic magnitudes for, respectively, the horizontal velocity components, the depth, and the gravity wave propagation speed in the model. Equations (11–13), when expressed in a time-space centered finite-difference form, are identical to those resulting from the expansion and linearization of eq (7–9).

By writing eq (11–13) in finite differences and assuming periodic solutions of the form $U_{i,j}^n=U^n\exp(F)$ with similar expressions for $V_{i,j}^n$ and $h_{i,j}^n$ where

$$F=\sqrt{-1}\,[ki\Delta x+lj\Delta y]$$

and superscript n refers to the time step, space dependence can be eliminated. The resulting equations are

$$U^{n+1}=U^{n-1}+(\hat{U}G+\hat{V}T)U^n+DV^n+\hat{C}Gh^n, \quad (14)$$

$$V^{n+1}=V^{n-1}-DU^n+(\hat{U}G+\hat{V}T)V^n+\hat{C}Th^n, \quad (15)$$

$$h^{n+1}=h^{n-1}+\hat{C}GU^n+\hat{C}TV^n+(\hat{U}G+\hat{V}T)h^n \quad (16)$$

where

$$G=-\sqrt{-4}\,B\sin\theta,$$

$$T=-\sqrt{-4}\,B\sin\alpha,$$

$$D=2f\Delta\pm,$$

$$B=\Delta t/\Delta x,$$

$$\theta=k\Delta x,$$

$$\alpha=l\Delta y,$$

k is the east-west wave number, and

l is the north-south wave number.

Equations (14–16) can be incorporated into a matrix form

$$\begin{pmatrix}U^{n+1}\\V^{n+1}\\h^{n+1}\\U^n\\V^n\\h^n\end{pmatrix}=A\begin{pmatrix}U^n\\V^n\\h^n\\U^{n-1}\\V^{n-1}\\h^{n-1}\end{pmatrix} \quad (17)$$

where A is the amplification matrix

$$\begin{pmatrix}\hat{U}G+\hat{V}T & D & \hat{C}G & 1 & 0 & 0\\ -D & \hat{U}G+\hat{V}T & \hat{C}T & 0 & 1 & 0\\ \hat{C}G & \hat{C}T & \hat{U}G+\hat{V}T & 0 & 0 & 1\\ 1 & 0 & 0 & 0 & 0 & 0\\ 0 & 1 & 0 & 0 & 0 & 0\\ 0 & 0 & 1 & 0 & 0 & 0\end{pmatrix}$$

The eigenvalues, λ, of this amplification matrix are the roots of the characteristic equation

$$[\lambda(L-\lambda)+1]^3=\lambda^2E^2[1+\lambda(L-\lambda)] \quad (18)$$

where

$$L=\hat{U}G+\hat{V}T$$

and

$$E^2=\hat{C}^2(G^2+T^2)-D^2.$$

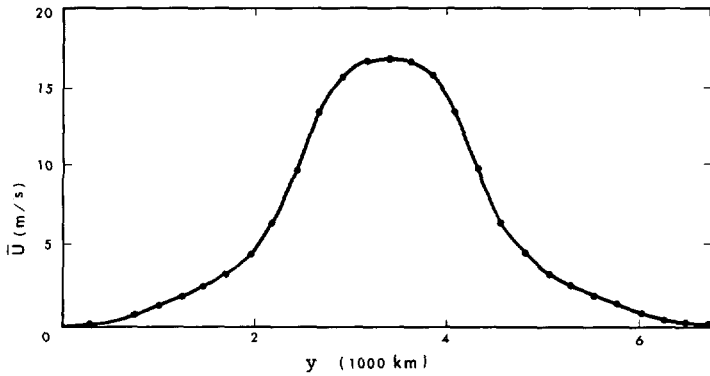There are two sets of unique roots to this sixth degree

FIGURE 1.—Zonally averaged fluid velocity distribution in the channel for the initial conditions; the abscissa is the distance from the northern boundary.

equation:

$$\lambda=\frac{(L\pm E)\pm[(L\pm E)^2+4]^{1/2}}{2} \tag{19}$$

and

$$\lambda=\frac{L\pm\sqrt{L^2+4}}{2}. \tag{20}$$

A necessary condition for stability is that the magnitude of all the eigenvalues be less than or equal to one. The conditions established by eq (20) are less restrictive than those of eq (19). There are two possible cases involving the radical in eq (19):

Case I in which $(L\pm E)>\sqrt{-4}$ that leads to $|\lambda|>1$ for all possible values of θ and α.

Case II in which $(L\pm E)\leq\sqrt{-4}$ that results in $|\lambda|\leq1$ for all possible values of θ and α.

Case II is of interest since case I will always give unstable conditions, while case II will produce, at worst, neutral stability. Expanding the terms in case II, one can write

$$B\left[\hat{U}+\hat{V}\pm\hat{C}\sqrt{2+\left(\frac{f\Delta x}{\hat{C}}\right)^2}\right]\leq1.$$

For this model,

$$\left(\frac{f\Delta x}{\hat{C}}\right)^2=.08$$

Since $(f\Delta x/\hat{C})^2\ll2$, one can use a binomial expansion to approximate the square root term to form a general stability criterion for a two-dimensional linearized form of the integration scheme used:

$$\sqrt{2}\frac{\Delta t}{\Delta x}\left[\left|\mathbf{V}\right|+\sqrt{g\hat{H}}\left(1+\frac{1}{4}\left(\frac{f\Delta x}{\hat{C}}\right)^2\right)\right]\leq1 \tag{21}$$

where $\mathbf{V}$ is a general velocity vector (magnitude $\sqrt{\hat{U}^2+\hat{V}^2}$) with components $\hat{U}$ and $\hat{V}$ assumed equal.
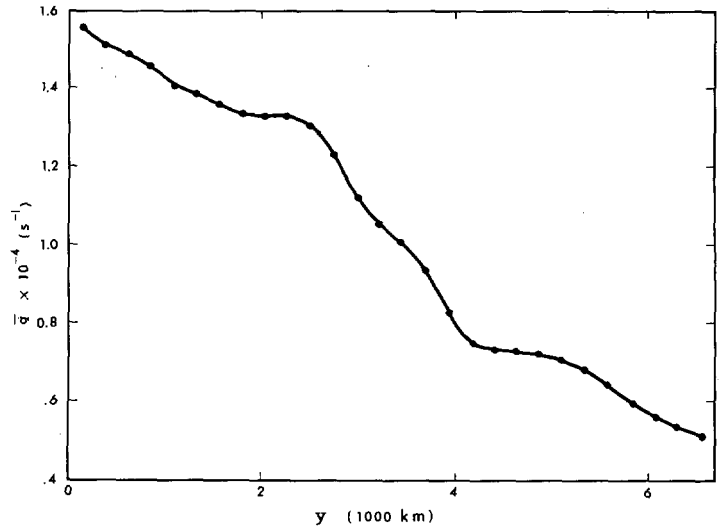

FIGURE 2.—Values of absolute vorticity, q, in the channel for the zonally averaged initial fluid velocity; the abscissa is the distance from the northern boundary.

Equation (21) agrees with the results of Richtmyer (1963) for the Lax-Wendroff scheme (1960) in two-space variables. For the parameters of this model, the term $(1/4)(f\Delta x/\hat{C})^2$ is much less than one and can safely be ignored.

Although computational stability may be assured by a careful choice of Δt, barotropic instability in the basic flow (as described in sec. 4) is also a possibility. The east-west zonal average of the U velocity, $\overline{U}$, for this flow is shown in figure 1.

For a nondivergent one-layer model, a necessary condition for barotropic stability is $\partial\overline{q}/\partial y=0$ (Pedlosky 1964) where $\overline{q}$ is the absolute vorticity defined as

$$\overline{q}=-\frac{\partial\overline{U}}{\partial y}+f.$$

Figure 2 shows the values of $\overline{q}$ for all values of y in the channel. Notice that q increases monotonically in the northward direction except for two locations where $\partial\overline{q}/\partial y\simeq0$. Also note that $\overline{q}>0$ which implies inertial stability. Wiin-Nielsen (1961) notes that, for westerly flow, stability is enhanced in the divergent model as compared to the nondivergent model for the same flow. Since the $\overline{U}$ field is at worst just marginally unstable according to the nondivergent criteria, for the divergent model the flow is most likely barotropically stable. Thus it is expected that a synoptic wave will remain a steady amplitude (or damped) Rossby wave in the absence of energy losses to unbalanced motions.

4. INITIALIZATION

For the experimental runs, the model is initialized by first prescribing the stream function, ψ, using the

relationship

$$\psi(x,y)=-\psi_0 \tan^{-1}\left[\frac{y-y_0-b\,\sin\dfrac{2\pi x}{L}}{d}\right] \qquad (22)$$

where

ψ_0 is the stream function amplitude factor;

y_0, the half width of the channel;

b, the north-south amplitude of the streamline through the jet axis;

d, a parameter that determines the width of the jet;

and

L, the basic east-west wavelength.

Values used were

$$\psi_0=1.44\times10^7\mathrm{m^2/s}, \qquad L=28\Delta s,$$
$$y_0=15\Delta s, \qquad d=2\Delta s,$$
$$b=3\Delta s, \qquad \text{and} \qquad \Delta s=240{,}000\ \mathrm{m}$$

which give a maximum fluid velocity of approximately 30 m/s in the center of the channel.

Since ψ must be a constant along the north-south boundaries, eq (22) is applied to within three grid points of these boundaries. The zonal average of the stream function at this point is then prescribed along each boundary. A linear gradient of stream function in the y direction is then prescribed for the remaining two points adjacent to the boundary.

Initial values of height, h, are calculated from the prescribed stream function using the balance relationship to suppress unwanted gravity waves. The balance relationship used is from Houghton et al. (1966) and may be written

$$\nabla^2 h=\frac{f}{g}\nabla^2\psi-\frac{2}{g}\left[\left(\frac{\partial^2\psi}{\partial x\partial y}\right)^2-\frac{\partial^2\psi}{\partial y^2}\frac{\partial^2\psi}{\partial x^2}\right]+\frac{\beta}{g}\frac{\partial\psi}{\partial y} \qquad (23)$$

where β is the constant beta parameter $\partial f/\partial y$. The right-hand side of eq (23) can be evaluated at all interior points in the channel model. However, for solving this type of equation for h, boundary values or normal gradients of h must be specified.

Average values of h on the northern boundary and southern boundary are prescribed so that the absolute value of the difference between the two boundaries is proportional to the total geostrophic mass flow in the channel and so that the mean depth is about 5000 m. Height variations along each boundary are computed according to the method of Stephens (1970) by the equation

$$g\frac{\partial h}{\partial x}=\frac{\partial\psi}{\partial x}\frac{\partial^2\psi}{\partial y^2}-\frac{\partial\psi}{\partial y}\frac{\partial^2\psi}{\partial x\partial y}-f\frac{\partial\psi}{\partial x}$$

that, for this case, can be simplified to

$$g\frac{\partial h}{\partial x}=-\frac{\partial\psi}{\partial y}\frac{\partial^2\psi}{\partial x\partial y}. \qquad (24)$$
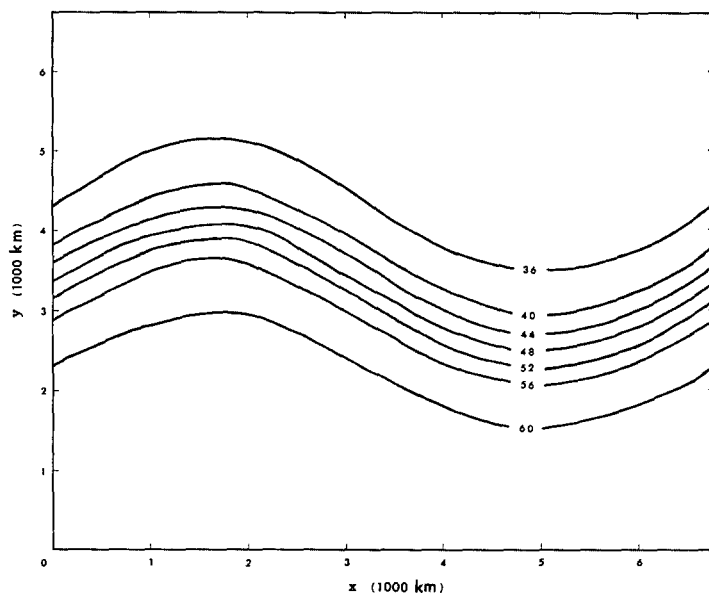

FIGURE 3.—Balanced initial height field (hundreds of meters) for experiment A; the ordinate is the distance from the southern boundary.

Figure 3 shows the resulting basic balanced height field used in this study.

Divergence, D, may be calculated from the prescribed stream function field using a quasi-geostrophic divergence relationship similar to that suggested by Phillips (1960):

$$\frac{g\bar h}{f}\nabla^2 D-fD+\left(\frac{\partial}{\partial x}\nabla^2\psi\right)\frac{\partial\psi}{\partial y}-\left(\frac{\partial}{\partial y}\nabla^2\psi\right)\frac{\partial\psi}{\partial x}$$
$$-\beta\frac{\partial\psi}{\partial x}+\frac{g}{f}\nabla^2\left(\frac{\partial\psi}{\partial x}\frac{\partial h}{\partial y}-\frac{\partial\psi}{\partial y}\frac{\partial h}{\partial x}\right)=0. \qquad (25)$$

Using the values of divergence obtained from eq (13), one may now calculate the velocity potential, χ, from $\nabla^2\chi=D$.

The U and V velocities can finally be obtained from the stream function and the velocity potential by the relationships

$$U=-\frac{\partial\psi}{\partial y}+\frac{\partial\chi}{\partial x}, \qquad V=\frac{\partial\psi}{\partial x}+\frac{\partial\chi}{\partial y}. \qquad (26)$$

All the previous equations involving the Laplacian operator, ∇^2, are solved using sequential relaxation techniques.

The time centered finite-difference equations require values of the variables U, V, and h at time t and $t-\Delta t$. However, for the first step, only one set of values (those at time $t_0=0.0$) is available. A forward step must be taken to produce values at $t_0+\Delta t$. The stability problems inherent in forward time stepping can be reduced if this first step is taken with reduced values of Δt. At time $t_0=0.0$, the initial forward step $\Delta t'$ is set equal to $\Delta t/8$. The next four centered time steps use successively doubled time steps until $\Delta t'=\Delta t$ is reached. Equal time steps are then used until the run is terminated.
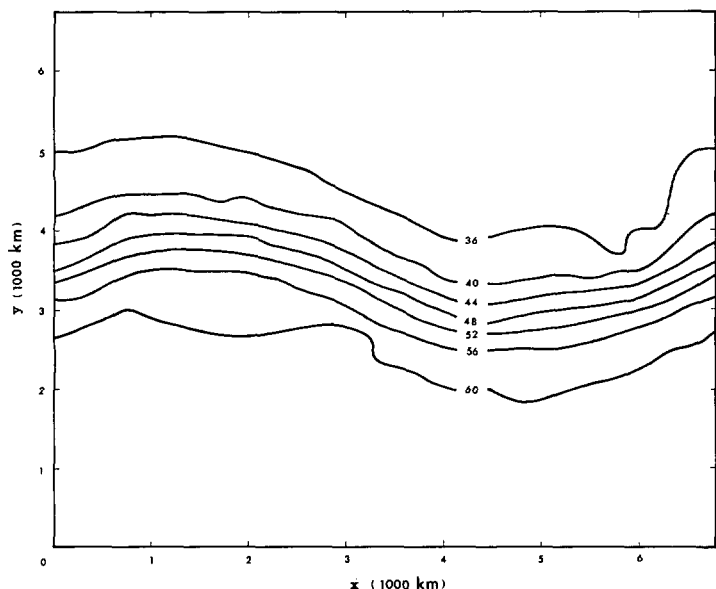
FIGURE 4.—Height field (hundreds of meters) after 5 model days for experiment A; note the short wavelength fluctuations and the decrease in longwave amplitude.
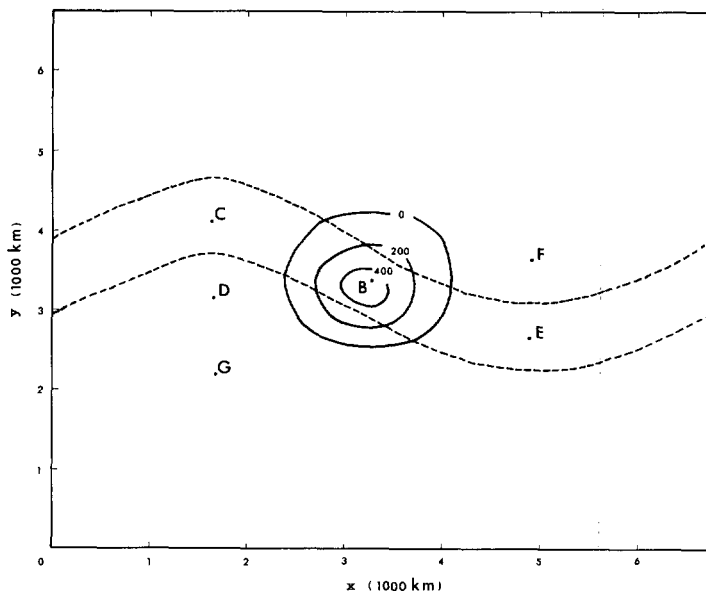

FIGURE 5.—Initial height perturbation for experiment B in meters (solid lines) and region of initial maximum fluid velocity from experiment A (dashed lines); perturbation center points are also shown for experiments C, D, E, F, and G.

5. NUMERICAL EXPERIMENTS

Seven experiments were conducted using a generally balanced basic synoptic flow. The dependent variables U, V, and h were determined initially from the prescribed stream function with the aid of the balance and quasi-geostrophic relationships as described in section 4. In the first experiment labeled "A," the height field shown in figure 3 was used for the initial condition. In the other experiments labeled "B" through "G," this initial height field was perturbed slightly.

The synoptic wave generated in experiment A (the unperturbed flow) was used as a standard of comparison for each succeeding experiment. Figure 4 shows the final height field after 5 model days. We see that the synoptic wave has developed small-amplitude, small-scale oscillations especially near the northern and southern boundaries. Also evident is the decrease in amplitude of the synoptic wave. These two effects are compatible. While total energy has remained unchanged, some of the synoptic wave energy has been transferred to small-scale fluctuations superimposed on the basic flow and some to the zonal flow. The small-scale fluctuations were very small initially, attesting to the suitability of the initializing procedures for the initially smooth and large-scale flow pattern in experiment A.

The wave appears to have retrograded slightly—less than one grid point, however. When applied to this flow at mid-channel, simple theoretical considerations give an eastward trace speed of -0.4 m/s, which after 5 days will produce a westward wave movement of two-thirds of a grid space. The basic synoptic scale wave is thus essentially stationary in theory and actuality for 5 days.

For experiments B through G, a perturbation height field was superimposed on the basic height field of experiment A. This local perturbation was determined by sinusoidal functions with a maximum amplitude of 10 percent of the basic height field at its center and a half width of about 500 km which is less than 10 percent of the wavelength of the fundamental wave. Figure 5 shows the initial height deviation or perturbation contours for experiment B and the location of the perturbation center for the remaining experiments. Experiments B, C, and E had the perturbation embedded in the core of maximum fluid velocity. Experiments D and F had this perturbation located on the edge of the main flow. In experiment G, the perturbation was well outside the main fluid velocity core. Only the height field is perturbed. The velocity field is left undisturbed. Note, therefore, that the height field is *not* balanced with the velocity field in the region of the perturbation.

Experiments B through G were allowed to proceed for 5 model days. At 3-hr intervals, the resulting height fields were compared to those of the standard, experiment A. All data are presented in height deviation form

$$(h_d)_{i,j} = (h_{ex})_{i,j} - (h_A)_{i,j}$$

where

$(h_{ex})_{i,j}$ is the height value of experiment (B, C, D, E, F, or G) at grid point i, j;

$(h_A)_{i,j}$ the height value of the standard, experiment A, at grid point i, j;

and

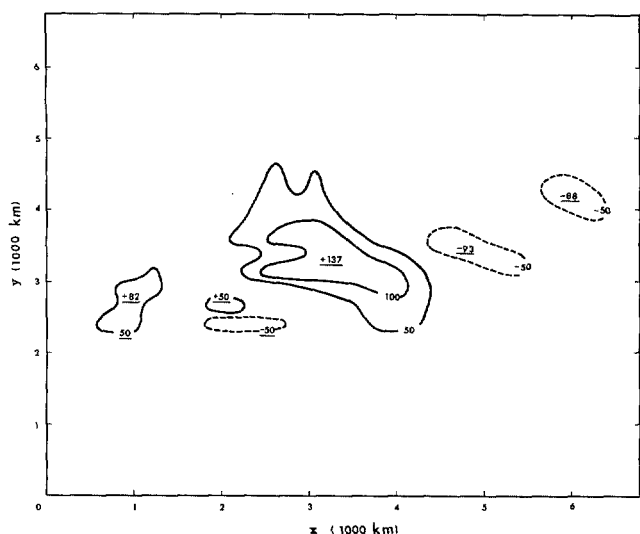$(h_d)_{i,j}$ the height deviation at grid point i, j.

FIGURE 6.—Perturbation height field in meters for experiment B after 5 days; the underlined values are center point magnitudes; positive perturbation contours are solid lines; negative contours are dashed; a time filtering has been used to eliminate the high-frequency oscillations as described in the text.
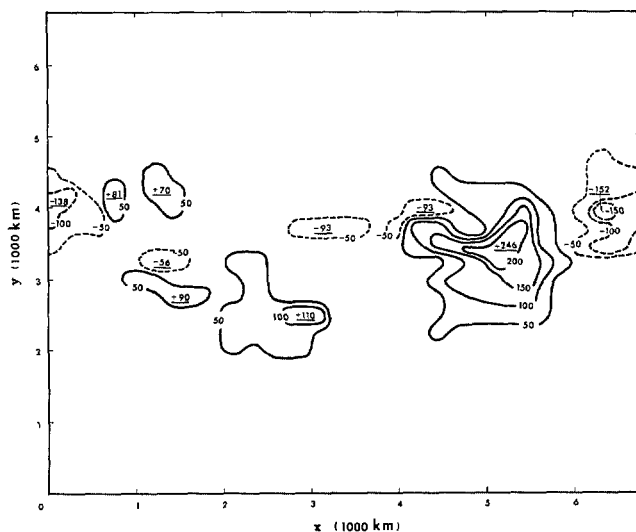

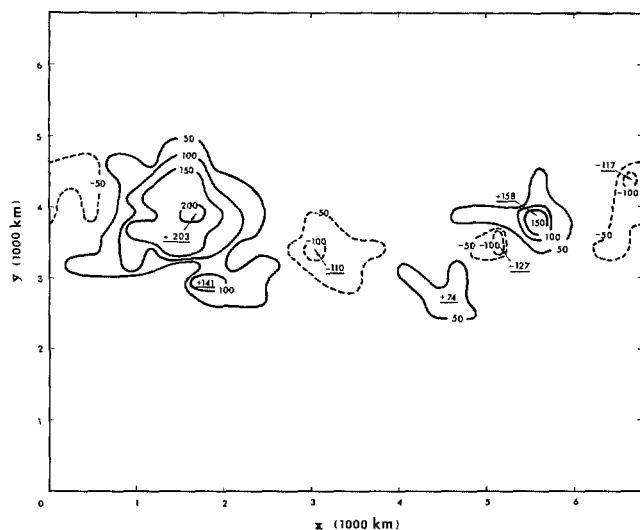FIGURE 9.—Same as figure 6, except this is for experiment E.

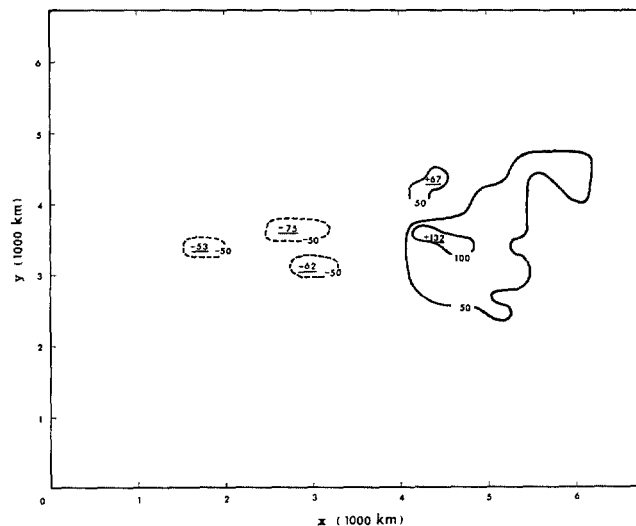FIGURE 7.—Same as figure 6, except this is for experiment C.

FIGURE 10.—Same as figure 6, except this is for experiment F.
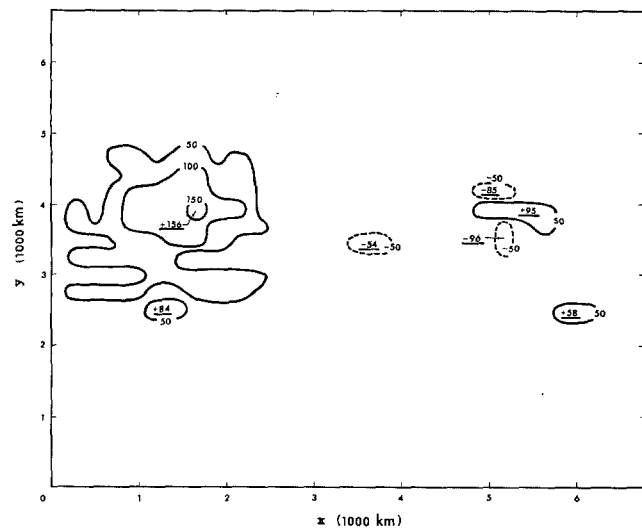

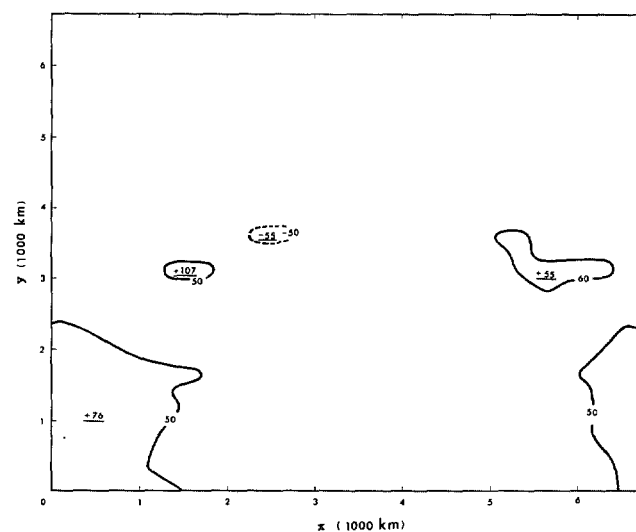FIGURE 8.—Same as figure 6, except this is for experiment D.

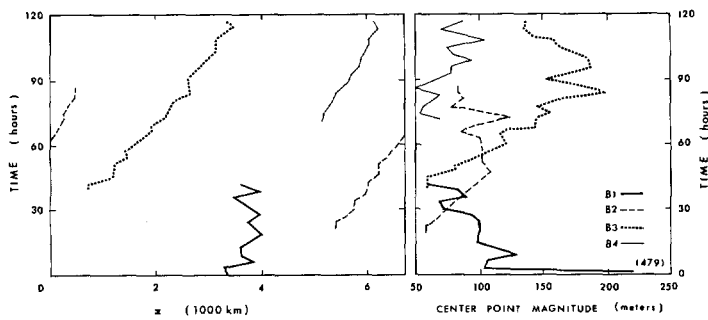FIGURE 11.—Same as figure 6, except this is for experiment G.

FIGURE 12.—East-west location and center-point magnitude for the principal perturbation groups in experiment B.
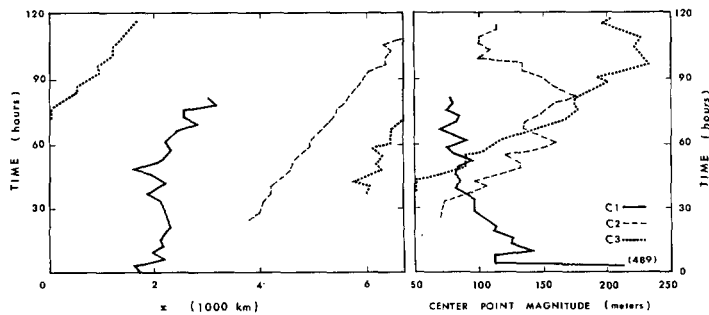

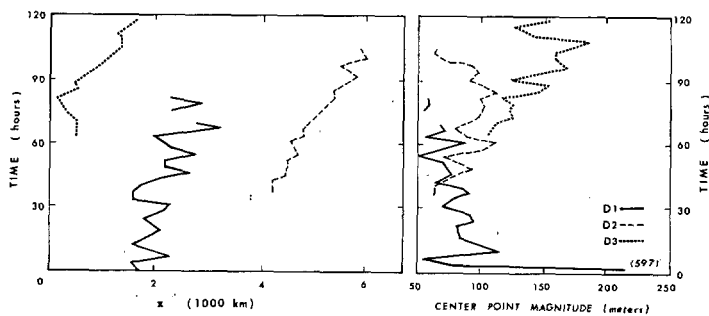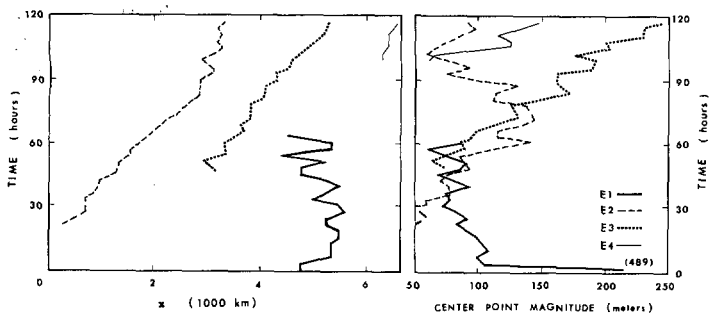FIGURE 16.—Same as figure 12, except this is for experiment F.

FIGURE 13.—Same as figure 12, except this is for experiment C.

FIGURE 17.—Same as figure 12, except this is for experiment G.

FIGURE 14.—Same as figure 12, except this is for experiment D.

FIGURE 15.—Same as figure 12, except this is for experiment E.
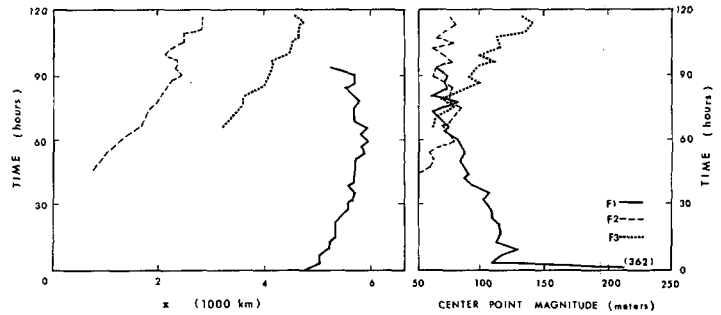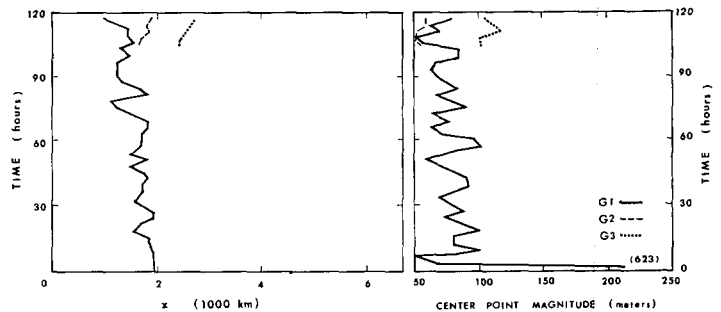
High-frequency height fluctuations from initial imbalances in experiments B through G tend to obscure the longer term fluctuations. A low pass filter, applied to the height deviation fields at output stage, reduced these short-term fluctuations significantly. The filter, a weighted average type, was of the form

$$(h_d)_{i,j}^t = 0.25(h_d)_{i,j}^{t-\Delta t} + 0.50(h_d)_{i,j}^t + 0.25(h_d)_{i,j}^{t+\Delta t}$$

where Δt was taken to be 3 hr. It must be emphasized that this low-pass filter was not allowed to interact with the model itself but was used to locate perturbations showing some degree of persistence. The resulting filtered height deviation fields (after 5 model days) are shown in figures 6-11 for experiments B through G.

The more persistent blocks of perturbations (>50 m in magnitude) were tracked at 3-hr intervals as they moved through the basic flow. Time tracks for these selected perturbation blocks are summarized in figures 12-17. The maximum deviation is also plotted for these blocks as a function of time. An estimate of the location, average speed, and maximum magnitude of each block is summarized in table 1 where each perturbation block is identified by a letter-number combination. The letter refers to the experiment, and the number to the order of appearance in the given experiment. The apparent origin of the block relative to the initial disturbance is determined by extrapolation from the earliest tracked location backward in time to $t=0$. A dash indicates the lack of a meaningful numerical value.

TABLE 1.—*Major perturbation disturbance blocks*

Perturbation block	Maximum attained height deviation (m)	Time, t_0, when height displacement first exceeds 50 m (hr)	Eastward velocity (m/s)	Apparent origin measured eastward from initial perturbation location (km)
B1	+479	0	—	0
C1	+489	0	—	0
D1	+597	0	—	0
E1	+489	0	—	0
F1	+362	0	—	0
G1	+623	0	—	0
B2	−125	21	8	1320
C2	−180	24	10	1320
D2	−116	36	7	1440
E2	−145	21	9	1320
F2	−87	45	8	1440
G2	−55	105	—	—
B3	+197	36	9	2640
C3	+232	36	8	2880
D3	+185	63	6	—
E3	+246	48	9	3120
F3	+141	66	8	2880
G3	+110	105	—	—
B4	−102	72	6	—
E4	−152	99	6	—

FIGURE 19.—Smoothed and normalized rms values for the height deviations in experiments B through G.
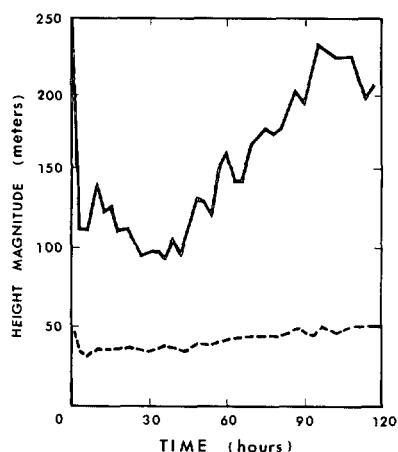

FIGURE 18.—Filtered rms values for the height deviations (dashed lines) and maximum perturbation center-point magnitude (solid lines) at 3-hr intervals for experiment C.

The height deviation fields were analyzed by calculating the root mean square (rms) values (after Lorenz 1969a) at 3-hr intervals for each experiment. When one uses the same notation as before, the rms value for experiments B through G at time t is

$$(\text{rms})^t_{ez} = \left\{ \frac{1}{MN} \sum_{i=1}^{M} \sum_{j=1}^{N} [(h_d)^t_{i,j}]^2 \right\}^{1/2}. \qquad (27)$$

The resulting time series of rms values were smoothed by a low-pass filter and are presented for experiment C in figure 18. For comparison with these rms values, the absolute value of the maximum height perturbation is
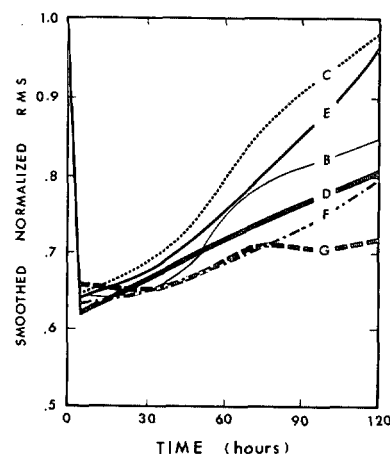
also shown in figure 18. The rms values were also normalized, filtered, and hand-smoothed for each experiment B through G. Figure 19 shows the resultant curves.

Disturbance energy was calculated for each experiment at each time step. Although very small fluctuations of disturbance energy could be seen (perhaps due to boundary effects), the total disturbance energy did not fluctuate by more than 0.1 percent for any experiment.

6. EXPERIMENTAL RESULTS AND CONCLUSIONS

The height deviation fields (discussed in sec. 5) when viewed sequentially for each experiment have many similar features. Table 1 shows the location and duration of the principal perturbation blocks.

During all experiments, the initial unbalanced height perturbation rapidly approaches balance with the fluid velocity field. During this process of about 6-hr duration, the center point magnitude decreases from about 500 to 100 m. This time factor depends on the horizontal space scale of the initial perturbation which is the same in all experiments in this study. This initial perturbation remains quasi-stationary and exhibits only a slight tendency to move with the main fluid flow. After the initial adjustment period, the center point magnitude slowly decreases until, after about 60 hr, the initial block is no longer discernible except in experiment G. This is consistent with elementary adjustment theory which predicts that the height field adjusts to the velocity field for a perturbation with a horizontal length scale less than the radius of deformation (defined $\hat{C}/f$) which is the case here.

After 21–45 hr, a second negative perturbation block appears downstream from the initial disturbance. In experiment G, this occurs much later. While growing rapidly, this block moves eastward at an average velocity of 8 m/s or about one-quarter of the maximum fluid velocity. This perturbation also begins to weaken after a time and even disappears after 5 days in three of the

experiments. If the motion of each of these perturbations is extrapolated backward in time to $t=0.0$ hr, this second perturbation originates at an apparent origin about 1300–1400 km east of the initial perturbation.

The third perturbation in all experiments is a positive one and first appears at 36–66 hr except much later in experiment G. This perturbation grows rapidly to $+200$ m or more and appears to have stopped growing when the model is terminated at 120 hr. This third block also moves eastward with a velocity of about 8 m/s. The apparent origin for the third block is generally from 2600–2700 km east of the initial perturbation for all experiments.

A fourth negative block appears in experiments B and E but does not appear in the others. The fourth block has the same general characteristics as the preceding blocks.

There are a few significant differences in the motion of all blocks for all experiments. There appear to be two types of response. Examining the initial appearance time, t_0, for the second and third blocks, one can contrast experiments B, C, and E with those of D, F, and G. There appears to be a 12-hr delay in the appearance of D2 as compared to B2, C2, and E2. This delay is longer for block F2 and longest for block G2. Similar conclusions hold for the third blocks.

A second differentiating characteristic is the maximum value of each perturbation. Again, the maximum values of B, C, and E are larger than D, F, and G for blocks 2 and 3. Block 1 is not considered since this information was specified initially. It appears from the above results that experiments B, C, and E have many similar characteristics, as do D, F, and G. It should be re-emphasized that perturbation blocks in experiments B, C, and E were located initially in the main fluid velocity core. The perturbation blocks in experiments D and F were only partially in this core while in G the initial perturbation block was entirely outside the core. The smoothed, normalized rms values for each experiment (fig 19) give additional support to this distinction. Again, rms values for B, C, and E are larger than D, F, and G after 45 hr.

One can easily be misled by these rms values, however, as can be seen from figure 18. The rms plot for experiment C is increasing slowly in time. A better picture of this growth can be seen from the dashed curve (maximum center point magnitude). Here, it is obvious that the maximum perturbation value more than doubles during the final 110 model hours while the rms value only increases by 50 percent during this same time period. The other four perturbation experiments showed similar results. The rms curve is thus a very conservative measure of the increase in magnitude of these traveling disturbances. The second curve in figure 18—maximum perturbation value—perhaps would be a better estimate of this growth.

The north-south motion of the perturbation blocks, while not analyzed in detail, shows uniform results. Traveling perturbation blocks tended to follow the north-south motion of the maximum fluid velocity core. In the experiments with the initial perturbation field located to one side of the fluid velocity core, the response indicated a gradual migration of this perturbation toward the jet core. The initial perturbation, quasi-stationary in nature, tended to be most persistant north of the synoptic trough and south of the ridge, especially in experiments D, F, and G. In experiment G, the initial perturbation remains as a nearly isolated anticyclonic gyre for the entire forecast period.

The traveling perturbations covered at least as much area in the horizontal plane as did the initial perturbation. The broadest (and most diffuse) perturbations developed in the initial perturbation in experiments D, F, and G after 20 model hours.

Thus, one can see that these perturbations or systematic errors superimposed on a stationary wave can, over a period of 5 days, lead to large traveling disturbances. The closer these disturbances are to the maximum fluid velocity core, the faster they grow. Perturbations injected into the flow, away from the main core, will also form traveling disturbances. However, in this case, they take an appreciably longer time to evolve. The most significant errors that develop away from the initial source region are always in or very near the jet stream axis. Care must be taken when initializing multiple-source data to a numerical model to reduce or at least monitor the effects of these systematic errors as they travel downstream at about 50 percent of the average fluid velocity.

The initial error results in high-frequency gravity waves and low-frequency quasi-geostrophic motions. Results of this study suggest that the latitudinal propagation of the low-frequency error fields is remarkably limited in the absence of fluid advection. This would be expected for Rossby wave motions of small scale in the absence of other wave motions. The interaction between the low-frequency error field and the large-scale motions is primarily limited to advection affects caused by the large-scale motions; however, other significant interactions are present. The high-frequency gravity wave motions have minimal interaction with the synoptic scale motions and can be properly sorted out by considering the time-averaged final computed solutions.

As a suggestion for further research, it would be valuable at this point to generalize these results to study the vertical propagation of these disturbances in a multilayer model. In such a model, one would expect a more continuous spectrum of motions in frequency space especially associated with error perturbations; and the resultant interactions with the basic synoptic scale flow could be far more intricate. Also desirable is the development of techniques for matching the direct and indirect data from multiple sources to reduce these systematic disturbances.

REFERENCES

Grammeltvedt, Arne, "A Survey of Finite-Difference Schemes foi the Primitive Equations for a Barotropic Fluid," *Monthly Weather Review*, Vol. 97, No. 5, May **1969**, pp. 384-404.

Houghton, David D., and Kasahara, Akira, "Non-Linear Shallow Fluid Flow Over an Isolated Ridge," *Communications on Pure and Applied Mathematics*, Vol. 21, No. 1, Jan. **1968**, pp. 1-23.

Houghton, David D., Kasahara, Akira, and Washington, Warren M., "Long-Term Integration of the Barotropic Equations by the Lax-Wendroff Method," *Monthly Weather Review*, Vol. 94, No. 3, Mar. **1966**, pp. 141-150.

Houghton, David, and Washington, Warren M., "On Global Initialization of the Primitive Equations: Part I," *Journal of Applied Meteorology*, Vol. 8, No. 5, Oct. **1969**, pp. 726-737.

Johnson, Michael H., "A Photogrammetric Technique for Finding Winds From Satellite Photos," *Studies in Atmospheric Energetics Based on Aerospace Probings, Annual Report*, Contract No. WBG-27, Department of Meteorology, The University of Wisconsin, Madison, **1967**, 231 pp. (see pp. 1-18).

Lax, Peter D., and Wendroff, Burton, "Systems of Conservation Laws," *Communications on Pure and Applied Mathematics*, Vol. 13, Interscience Publications, Inc., New York, N.Y., **1960**, pp. 217-237.

Lorenz, Edward N., "Atmospheric Predictability as Revealed by Naturally Occurring Analogues," *Journal of the Atmospheric Sciences*, Vol. 26, No. 4, July **1969a**, pp. 636-646.

Lorenz, Edward N., "The Predictability of a Flow Which Possesses Many Scales of Motion," *Tellus*, Vol. 21, No. 3, Stockholm, Sweden, Aug. **1969b**, pp. 289-307.

Pedlosky, Joseph, "The Stability of Currents in the Atmosphere and the Ocean: Part I," *Journal of the Atmospheric Sciences*, Vol. 21, No. 2, Mar. **1964**, pp. 201-219.

Phillips, Norman A., "On the Problem of Initial Data for the Primitive Equations," *Tellus*, Vol. 12, No. 2, Stockholm, Sweden, May **1960**, pp. 121-126.

Richtmyer, Robert D., "A Survey of Difference Methods for Non-Steady Fluid Dynamics," *NCAR Technical Notes* 63-2, National Center for Atmospheric Research, Boulder, Colo., **1963**, 25 pp.

Rossby, Carl Gustav, "On the Mutual Adjustment of Pressure and Velocity Distributions in Certain Simple Current Systems, II," *Journal of Marine Research*, Vol. 1, No. 3, Sept. 20, **1938**, pp. 239-263.

Shuman, Frederick G., "Numerical Experiments With the Primitive Equations," *Proceedings of the International Symposium on Numerical Weather Prediction, Tokyo, Japan November 7-13, 1960*, Meteorological Society of Japan, Tokyo, Mar. **1962**, pp. 85-107.

Smagorinsky, Joseph, "Problems and Promises of Deterministic Extended Range Forecasting," *Bulletin of the American Meteorological Society*, Vol. 50, No. 5, May **1969**, pp. 286-312.

Smith, William L., "An Iterative Method for Deducing Tropospheric Temperature and Moisture Profiles From Satellite Radiation Measurements," *Monthly Weather Review*, Vol. 95, No. 6, June **1967**, pp. 363-369.

Stephens, J. J., "Variational Initialization With the Balance Equation," *Journal of Applied Meteorology*, Vol. 9, No. 5, Oct. **1970**, pp. 732-739.

Wiin-Nielsen, A., "On Short- and Long-Term Variations in Quasi-Barotropic Flow," *Monthly Weather Review*, Vol. 89, No. 11, Nov. **1961**, pp. 461-476.